

An Effective Multivector Model Predictive Current Control for PMSM Drive based on Low-Complexity Voltage Vector Preselection

Parvathy M.L.^{1,2}, and Vinay Kumar Thippiripati¹, *Senior Member, IEEE*

¹Department of Electrical Engineering, National Institute of Technology, Warangal, India-506004.

²Department of Engineering, Durham University, United Kingdom, DH1 3LE.

Abstract— Model Predictive Current Control (MPCC) is an advanced control strategy for non-linear constrained systems that demand quick dynamic response. An effective multivector MPCC technique based on a low-complexity voltage vector (VV) preselection is proposed in this article for the PMSM drive. The proposed scheme employs three vectors in a sample time as the single VV application leads to large fluctuations in torque. As the application of multiple VVs augments the complexity of the algorithm, the proposed scheme opts for the principle of current error minimization as a criterion for VV preselection. Hence, the proposed MPCC technique employs the previous sample VV and the motor rotation direction as parameters for preselection, thereby limiting the computations using a set of four VVs. Moreover, the application of multiple VVs is achieved using a gradient-based approach, selecting the first optimum VV from the preselected set and determining the suitable adjacent VV as the second optimum VV through voltage error gradients. Application times are then precisely determined using the deadbeat concept, effectively reducing the steady-state torque fluctuations without compromising dynamic response. Further, the proposed control algorithm is comprehensively compared with basic MPCC and recent literature to ensure its effectiveness.

Index Terms—multiple vectors, PMSM, computational time reduction, two-level VSI.

I. INTRODUCTION

Out of the total energy generated globally, at least 50% is converted into mechanical energy for agricultural, transportation, domestic, and industrial applications [1]. In industries, electric motors act as the major load and utilize around 70% of the generated electricity [2]. Consequently, it is crucial to deploy highly efficient electric motors for better energy consumption. Permanent Magnet Synchronous Motor (PMSM) [3] is experiencing rapid growth in the realm of adjustable speed drives, owing to its enhanced efficiency, expansive speed range operability, compact dimensions, and a remarkable torque-to-inertia ratio. In transportation and industrial applications, there is a stringent requirement for sophisticated control strategies offering high dynamic performance. The control strategies that have been dominating the drives sector for the past few decades are Direct Torque Control (DTC) and Field-oriented control (FOC) [4]. The DTC scheme provides excellent dynamic performance, while the FOC scheme ensures enhanced steady-state performance. However, FOC has a sluggish dynamic response and DTC has a poor steady-state response affected by large fluctuations in torque and flux [5].

Model predictive control (MPC) is a non-linear control

technique that is rapidly finding its base in the power electronics and drives area. The concept of MPC was originally introduced for process control in the petrochemical industry. Although the scheme has undergone several improvements and has a wider research interest globally [6], its product-level realization in the drive application is under scrutiny owing to computational intensity. With the progression in semiconductor device technology and the availability of powerful digital processors, MPC schemes are expected to be extensively utilized for real-time drive applications in the near future.

The MPC schemes are popularly categorized as Model Predictive Torque Control (MPTC) and Model Predictive Current Control (MPCC). In MPCC, the cost function uses the stator current errors as the control variables [7]. Hence, the estimation of the torque and flux can be avoided in the MPCC scheme. Furthermore, the difficulty in evaluating the weighting factors in the MPTC scheme can be circumvented with the help of the MPCC method [8]. Thus, the computational burden incurred during the implementation of the MPCC algorithm is less.

In MPCC, the optimum vector is applied for the complete sample period and since the current error is not meticulously restrained to its minimum value, there would be a degradation in the flux and torque response [9]. Moreover, in a 2-level-VSI (2L-VSI), the control set comprises merely eight voltage vectors (VV) with constant magnitude and phase. With fewer VVs in the control set, there is a limited degree of freedom of control, yielding large flux and torque fluctuations. This is particularly noticeable when the sample duration is large. Thus, the key downside of the MPCC scheme is the large fluctuations in flux and torque prompted by the utilization of a single optimum VV for an entire control interval [10]. This limitation is addressed using duty modulation schemes. However, the majority of existing duty schemes rely on complex computations that count on the precision of the involved machine parameters [11]. The computational burden is also augmented due to the additional calculations involved in these schemes [12].

To consider the limitation of the higher computational burden associated with the predictive control algorithms, several research works propose effective preselection of VVs used for shortlisting the optimum VV [13]. The VV preselection is designed to prioritize only those VVs with a more pronounced impact on the control objectives. In addition, the steady-state drive response can be enhanced using dual VVs [14] or two

active and null VV [15] applications. In [16], a VV preselection is employed to bring down the number of VVs from 8 to 4. Even though the computational burden is reduced, there is a chance to select sub-optimal VVs in certain control intervals. In [17], the VVs are selected using the current vector location, and the optimal VV amplitude is optimized by adding a null VV. In [18], the reference VV is calculated to shortlist the optimum VV. Two active VVs or one active and a null VV are applied to effectively reduce the torque variations. However, the proposed scheme requires complex tangent inverse angle calculations for sector determination. The reference VV calculation also induces some parameter sensitivity into the algorithm.

In several conditions, the application of null VV alone cannot effectively bring down the stator current error. In such cases, multiple VVs, i.e., null VV along with two active VVs or even three active VV application schemes are considered to alleviate the steady-state ripples [19]. Nevertheless, this enlarges the execution time of the predictive algorithm and increases the switching frequency. In [20], the control algorithm suitably selects an active or null vector as the next optimum VV. Nevertheless, this method is limited due to the large computational time.

A multivector application is achieved in [21] and [22], using amplitude-optimized extended control set-based VVs. The virtual VV concept is used to extend the control set and improve the control precision of the algorithm. The extended control set-based MPCC schemes offer a better response at the outlay of enlarged computational time. To reduce the inverter switching frequency, adjacent VVs are employed in [23] according to the number of transitions in switching states. The optimal VV that generates minimum switching state transition is applied for meeting the target objective. In [24], the reduced switching frequency is obtained using a duty-ratio correction technique. The weighting factor is tuned online to achieve the required performance. In [25], a modulation technique is proposed for the 5-phase PMSM drive. The virtual VV concept is used to alleviate the harmonics and for reducing the computational time of the algorithm a VV preselection scheme is proposed. Several research works also utilize look-up tables framed based on the errors to suitably preselect the VVs to be used for the evaluation of optimum VV. In [26], a 3D look-up table is used for the preselection and the inverter switching time is determined with the help of the space vector modulation method. However, the execution time is increased in this method. In [27], a low-complexity multivector scheme is proposed which uses only 3 VVs for the evaluation of optimum VV. However, the duty ratio control takes up a lot of computational time. Thus, the available multivector schemes are either computationally complex [28] or require the determination of additional parameters. This motivates the implementation of a low-complexity VV selection-based multivector MPCC with improved torque response.

In recent years, Model-Free Predictive Control (MFPC) has been developed to reduce reliance on physical models, utilizing only the input and output data of the system [29]. Meanwhile, extending the prediction horizon has been shown to enhance the performance of MPCC schemes. However, this improvement

comes at the cost of increased computational complexity. To address this, a fully scalable Sphere Decoding Algorithm (SDA) is proposed in [30], enabling the use of longer prediction horizons. In [31], a low-complexity MPCC scheme based on the deadbeat principle is introduced for an Open-End Winding PMSM (OEW-PMSM) drive, employing reference VV calculation through a 3D analysis to select VVs efficiently. Similarly, a cascaded predictive control scheme with low computational demands is proposed in [32] for OEW-PMSM drives. In [33], another VV-based control strategy utilizing virtual VVs is implemented for a five-level OEW-PMSM drive, aiming to reduce computational effort. Additionally, [34] presents a double VV application method to enhance the steady-state performance of a five-phase PMSM drive, leveraging a deadbeat strategy to shortlist VVs and lower computational costs. Another implementation in [35] uses a double VV application to improve steady-state performance, but requires additional processing for selecting the second VV with minimal switching transitions. Further, a reference VV tracking-based MPC scheme is proposed in [36], using a 2D planar model to further reduce computational complexity in the control algorithm.

The current work proposes an effective multivector MPCC technique for the 2L-VSI-fed PMSM drive based on a low-complexity VV preselection scheme. The main contribution of the proposed scheme is that the VVs are preselected based on the principle of stator current error minimization and require only the reference speed and the previous sample VV for the VV grouping. The number of VVs used to evaluate the optimum VV is reduced from 8 to 4 in the proposed method. The VVs are grouped in such a way as to address all the stator current error conditions. It avoids sector determination and reference VV calculation to limit the computational burden while applying multiple VVs for steady-state torque performance improvement. In the proposed MPCC, three VVs are applied in each control period. After the evaluation of the cost function using VVs in the preselected group, the first VV is shortlisted and the second optimum VV is obtained using an improved position evaluation method. The gradient of the voltage error is used for estimating the second optimum VV. Moreover, the deadbeat control scheme is used to find the duration of application of the optimum VVs. Furthermore, the proposed MPCC retains the dynamic performance offered by the basic MPCC (BMPCC) and it offers a lesser computational time compared to recent literature with improved steady-state torque response. The proposed work is relevant because it addresses a key challenge in BMPCC schemes, i.e., balancing high control performance with low computational complexity. Moreover, multivector based MPCC scheme often require intensive computations due to the evaluation of all possible voltage vectors, which can limit their suitability for real-time applications, especially in systems with fast dynamics or limited processing power.

The article has the following organization: The mathematical model of PMSM is given in Section I. Section III broadly describes the proposed scheme. The experimental results and the conclusion are described in sections IV and V of the article,

respectively.

II. DYNAMIC MODELLING OF PMSM

The stationary frame model of the surface-mounted PMSM can be framed as per the equations given below.

$$u_s = i_s R_s + \frac{d\psi_s}{dt} \quad (1)$$

$$\psi_s = L_s i_s + \psi_r \quad (2)$$

where the stator voltage and the stator flux are denoted as u_s and ψ_s , respectively. Let L_s indicate the stator-inductance, and R_s be the stator-resistance. Correspondingly, the stator current be i_s , and the pole pair be symbolized as p . Let w_r and ψ_f be denoting the electrical speed, and the permanent magnet flux, respectively, where, the rotor flux is $\psi_r = \psi_f e^{j\theta}$.

Using (2) in (1) and rearranging, the state space representation equation can be represented as,

$$\frac{di_s}{dt} = \frac{1}{L_s} (u_s - R_s i_s - j w_r \psi_r) \quad (3)$$

The electromagnetic-torque (T_e) can be estimated using (4).

$$T_e = \frac{3}{2} p (\text{imag}(\overline{\psi_s} \times i_s)) \quad (4)$$

III. PROPOSED MPCC METHOD

A. Basic Model Predictive Current Control

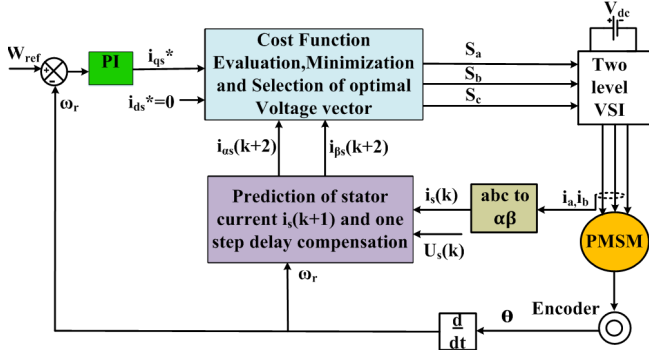


Fig.1. Block diagram of basic MPCC scheme.

Fig. 1 shows the schematic of the basic MPCC (BMPCC) scheme. In BMPCC, the cost function (G) has current error terms formulated using the currents along the stationary α -axis (i_{as}) and β -axis (i_{bs}). The stator flux and torque control can be achieved using the control of i_{as} and i_{bs} .

$$G = ||i_s^* - i_s(k+1)||^2 \quad (5)$$

The stator current behavior can be predicted using the current equation given in (3) evaluated through a set of eight possible VVs in the 2L-VSI.

$$i_s(k+1) = i_s(k) + \frac{T_s}{L_s} (U_s(k) - i_s(k)R_s - j\psi_r w_r e^{j\theta}) \quad (6)$$

where, the predicted current, $i_s(k+1) = i_{as}(k+1) + j i_{bs}(k+1)$.

The delay inherited during the digital implementation of the control algorithm can be overcome using the delay compensation technique. This modifies the cost function as,

$$G = ||i_s^* - i_s(k+2)||^2 \quad (7)$$

The BMPCC scheme evaluates the cost function repeatedly in every control interval according to the number of switching

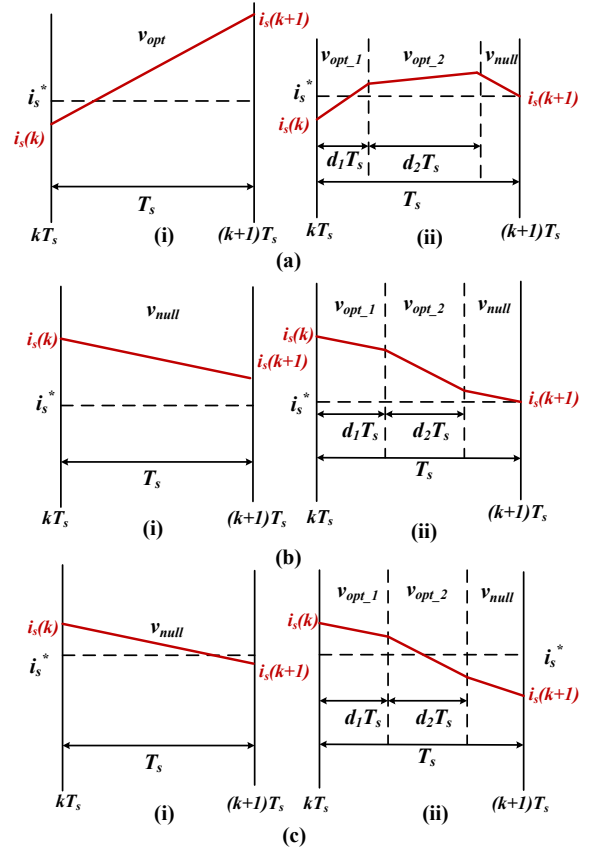


Fig.2. Current trajectory when (i) one VV is applied and (ii) multiple VVs are applied under the conditions: (a) the deviation between the assessed current and the reference value is negative (b) the deviation between the assessed current and the reference value is positive with a substantial initial magnitude of error (c) the deviation between the assessed current and the reference value is positive with a trivial initial magnitude of the error.

states of the VSI. In the 2L-VSI control set, out of the eight vectors, the VV that yields the minimum cost function value is selected as the optimum vector. However, the optimum VV is not applied on the basis of the error magnitude, which generates more fluctuations in the responses of torque and flux. To address this drawback of BMPCC, dual or multiple VV-based control schemes are widely researched. The typical stator current trajectory during a control period can be depicted as shown in Fig.2. The slope of the currents in Fig.2 may not be precise as it is purely used for illustration. It can be observed that the single VV-based control causes large stator current fluctuations. The reference current can be either greater than or less than the estimated current in any control period. For example, if the assessed current value is less than its reference value, as shown in Fig. 2(a), the single VV application will lead to a larger ripple. However, when we apply two active VVs with a rising slope in that particular instant along with the null VV, the ripple magnitude can be effectively brought down. Correspondingly, with a large error at the initial instant, when the sensed value of current is higher than its reference value, two active VVs with a falling slope along with the null vector can reduce the ripple as given in Fig. 2(b). However, when the error at the initial instant is insignificant, the application of the null VV itself is sufficient to bring down the error. Thus, it is relevant to suitably apply the VVs based on the magnitude of

the VVs is directly evaluated without using the space vector modulation technique. The proposed VV grouping aids in reducing the number of VVs used for the computations from 8 to 4. This ensures a reduced computational complexity while applying multiple VVs. Therefore, after the evaluation of the cost function and optimization stages with the four VVs in the VVG, the VV that produces the minimum current error is selected as the first VV. Moreover, the VV placed adjacent to the first VV is preferred as the second active VV. Nevertheless, every VV has two adjacent VVs, and the best choice out of the two is obtained using the stator voltage error position. Using the discretized stator current equation in (3) and neglecting the stator resistance,

$$\Delta i_s = i_s^* - i_s(k+1) = (U_s^* - e(k+1)) \frac{T_s}{L_s} \quad (8)$$

where, $\Delta i_s = \Delta i_{\alpha s}(k+1) + j\Delta i_{\beta s}(k+1)$, is the stator current error. The stator current error thus holds a linear relation with the reference VV (U_s^*). Thus, for easy determination of the second optimum VV, it is sufficient to determine the position of voltage error, Δv , which can be obtained from (8) as,

$$\Delta v = \frac{\Delta i_s}{k} \quad (9)$$

where, $k = T_s/L_s$, a constant. The position of Δv with respect to the first optimum VV, V_{opt1} , can be obtained using the gradient. Let Δv_{grad} be the gradient of the voltage error. It can be obtained as,

$$\Delta v_{grad} = \frac{\text{imag}(\Delta v)}{\text{real}(\Delta v)} \quad (10)$$

The second VV, V_{opt2} , is selected as the VV ahead of V_{opt1} , if Δv_{grad} is greater than the gradient of V_{opt1} . Similarly, V_{opt2} is chosen as the VV behind V_{opt1} , if Δv_{grad} is less than the gradient of V_{opt1} . This VV selection criterion is summarized in the following equation.

$$V_{opt2} = \begin{cases} V_{opt1} + I, & \text{if } \Delta v_{grad} \geq (\text{imag}(V_{opt1})/\text{real}(V_{opt1})) \\ V_{opt1} - I, & \text{if } \Delta v_{grad} < (\text{imag}(V_{opt1})/\text{real}(V_{opt1})) \end{cases} \quad (11)$$

For achieving the multivector application, the extent of application of the VVs must be determined. The proposed method utilizes the deadbeat concept to evaluate the duty ratios of the optimum VVs as shown in Fig. 6. Assuming the duty ratios of V_{opt1} , V_{opt2} , and null VV as d_1 , d_2 , and d_0 , respectively, the sum of duty ratios can be obtained as,

$$d_1 + d_2 + d_0 = 1 \quad (12)$$

Using the deadbeat principle, assuming that the predicted current reaches the reference value at the $(k+2)^{\text{th}}$ instant, we get,

$$i_{\alpha s}(k+2) = i_{\alpha s}^*(k+2) \quad (13)$$

$$i_{\beta s}(k+2) = i_{\beta s}^*(k+2) \quad (14)$$

If the average voltage applied during a sample time T_s is equal to the voltage error Δv , we get,

$$\Delta v_{\alpha} = d_1 V_{opt1\alpha} + d_2 V_{opt2\alpha} \quad (15)$$

$$\Delta v_{\beta} = d_1 V_{opt1\beta} + d_2 V_{opt2\beta} \quad (16)$$

Solving (15) and (16), we get,

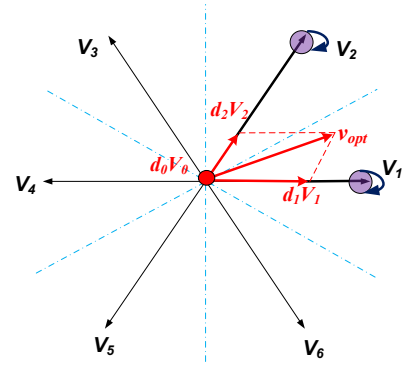


Fig. 6. Determination of optimum VV using two active and a null VV.

$$d_1 = \frac{\Delta v_{\beta} V_{opt2\alpha} - \Delta v_{\alpha} V_{opt2\beta}}{V_{opt2\alpha} V_{opt1\beta} - V_{opt1\alpha} V_{opt2\beta}} \quad (17)$$

$$d_2 = \frac{\Delta v_{\beta} V_{opt1\alpha} - \Delta v_{\alpha} V_{opt1\beta}}{V_{opt1\alpha} V_{opt2\beta} - V_{opt2\alpha} V_{opt1\beta}} \quad (18)$$

$$d_0 = 1 - d_1 - d_2 \quad (19)$$

Thus, the duty ratios of the optimum VVs can be found using (17)-(19). The constant value (k) is predetermined and the value of the current error is divided with it for the determination of Δv . Thus, additional parameter evaluation can be avoided for the determination of the optimum duration of active VVs. The proposed scheme ensures the optimum VV selection due to the grouping of VVs to address all error conditions. The proposed duty modulation scheme is simple and offers improved torque response through the multiple VV application. The proposed scheme can be illustrated using the flow chart shown in Fig. 7.

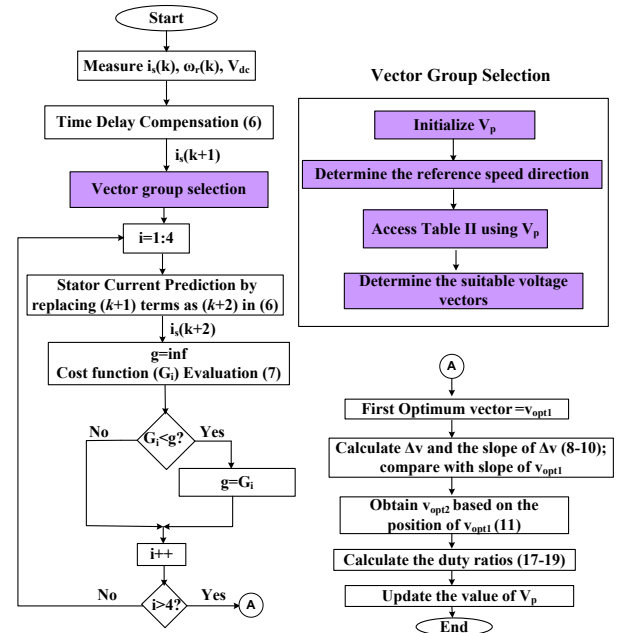


Fig. 7. Flow chart of the proposed MPCC scheme.

IV. EXPERIMENTAL VALIDATION

A. Hardware Description

The experimental validation is performed in a 415 V, 5 hp, 1500

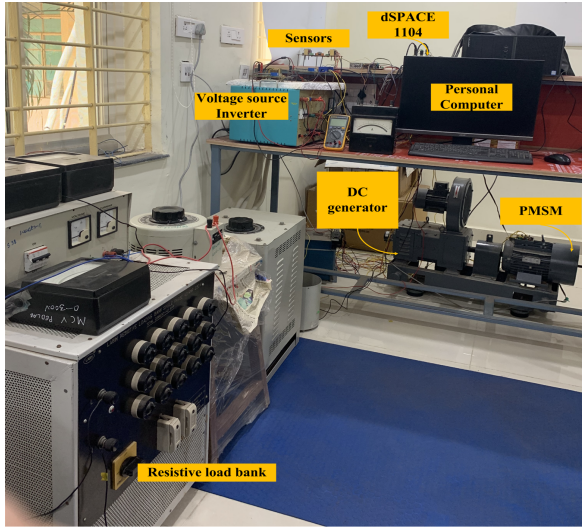


Fig.8. Experimental setup.

Table-II. PMSM parameters

Parameters	Value
Rated Power (hp)	5
No. of poles	4
R_s (ohm)	1.12
Rated speed (rpm)	1500
L_s (H)	0.105
Ψ_f (Wb)	1
Rated Current (A)	6

rpm, 4 pole, PMSM machine. The algorithms are developed using MATLAB/SIMULINK interfaced with a dSPACE 1104 control platform. Hall effect sensors are utilized for estimating the DC-link voltage and currents. The incremental encoder with a 1024-point resolution is used for the speed feedback. The electrical loading is offered using a DC machine attached to the PMSM shaft. Fig.8 shows the hardware setup used for all the performance investigations. The motor parameters are specified in Table II.

The performance of the proposed MPCC method is evaluated using the comparison of steady-state and dynamic performance with BMPCC, duty-based MPC[18] (DBMPC [18]), and multi vector-based MPC[27] (MVBMPCC [27]) scheme. All the methods are subjected to the same operating conditions while maintaining a sampling frequency of 10 kHz. The DBMPC [18] scheme uses two VVs in every control period and the evaluation of the optimum VV is obtained from a reference VV-based selection scheme. Even though the VVs used for the computations are reduced to two, the estimation of sectors using

tangent inverse angle calculation takes up a considerable amount of computational time. In the MVBMPCC [27] scheme, three VVs are applied in a control interval and only three VVs are used for computations pertaining to optimum VV determination. However, the duty-ratio determination comprises more calculations.

B. Evaluation of steady-state and dynamic performance

The control algorithm response is evaluated under steady-state and dynamic conditions to establish its effectiveness. The machine is subjected to work at different ranges of speed to assess its steady-state performance. Fig.9 shows the drive response at a speed of 500 rpm under no-load conditions. Further, the steady-state response is determined at a medium speed of 750 rpm is shown in Fig.10. The motor performance is further evaluated at speeds of 500 rpm with 5 Nm load, and 1000 rpm with 12 Nm load as presented in Fig. 11 and Fig.12, respectively. The speed, torque, flux, and current waveforms obtained are shown in every response. Moreover, the steady-state response of the proposed scheme is compared with a deadbeat SVM (DBSVM [28]) method in Fig. 13. The DBSVM[28] scheme offers improved performance at the expense of enlarged complexity in implementation and increased switching frequency. For a fair comparison, the steady-state drive performance at 1000 rpm and 10 Nm load when operated at a similar switching frequency of 4.5 kHz is analyzed as shown in Fig. 14. It can be observed that the proposed scheme offers better steady-state performance when operated at a similar switching frequency compared to DBSVM[28], MVBMPCC[27] and DBMPC[18] schemes. The standard deviation is used to determine the torque fluctuations (T_{er}), and flux fluctuations (Ψ_{er}),

$$T_{er} = \sqrt{\frac{1}{n} \sum_{i=0}^n (T_e(i) - T_e^*)^2} \quad (27)$$

$$\Psi_{er} = \sqrt{\frac{1}{n} \sum_{i=0}^n (\Psi_e(i) - \Psi_e^*)^2} \quad (28)$$

The average switching frequency (f_s) of the inverter is calculated using the number of switching (n_s) within a time period (t_p), as given below.

$$f_s = \frac{n_s}{6t_p} \quad (29)$$

The proposed MPCC scheme responses are thus evaluated at different speeds and different load conditions.

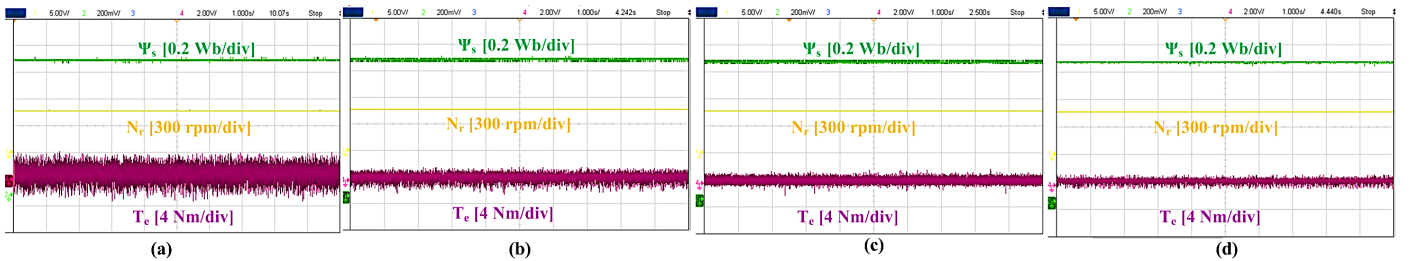


Fig.9. Steady-state drive performance at 500 rpm speed (a) BMPCC, (b) DBMPC[18], (c) MVBMPCC[27], (d) Proposed MPCC

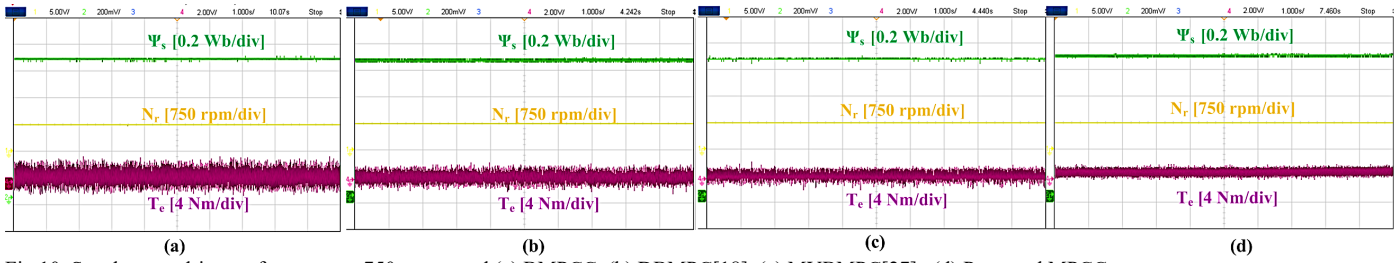


Fig.10. Steady-state drive performance at 750 rpm speed (a) BMPCC, (b) DBMPC[18], (c) MVBMPCC[27], (d) Proposed MPCC.

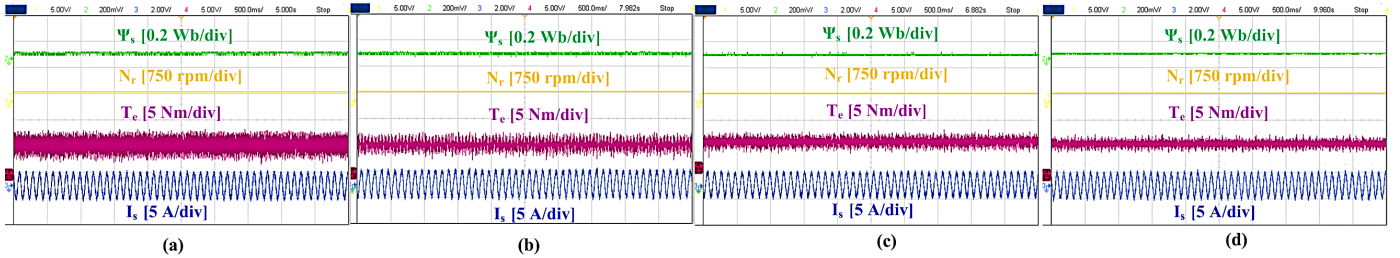


Fig.11. Steady-state drive performance at 500 rpm speed and 5 Nm load (a) BMPCC, (b) DBMPC[18], (c) MVBMPCC[27], (d) Proposed MPCC.

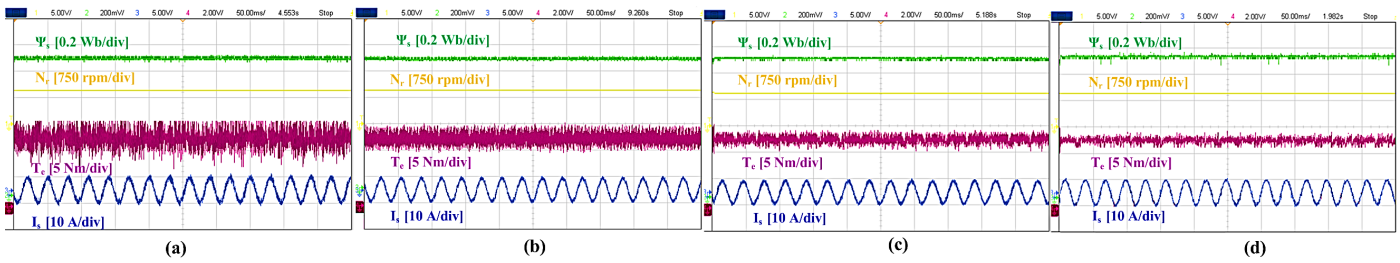


Fig.12. Steady-state drive performance at 1000 rpm speed and 12 Nm load (a) BMPCC, (b) DBMPC[18], (c) MVBMPCC[27], (d) Proposed MPCC.

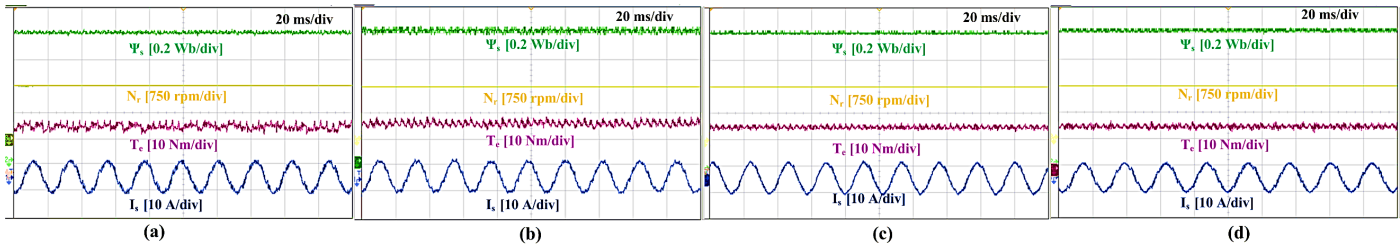


Fig.13. Steady-state drive performance at 1500 rpm and 15 Nm load (a) DBMPC[18], (b) MVBMPCC[27], (c) DBSVM [28] (d) Proposed MPCC.

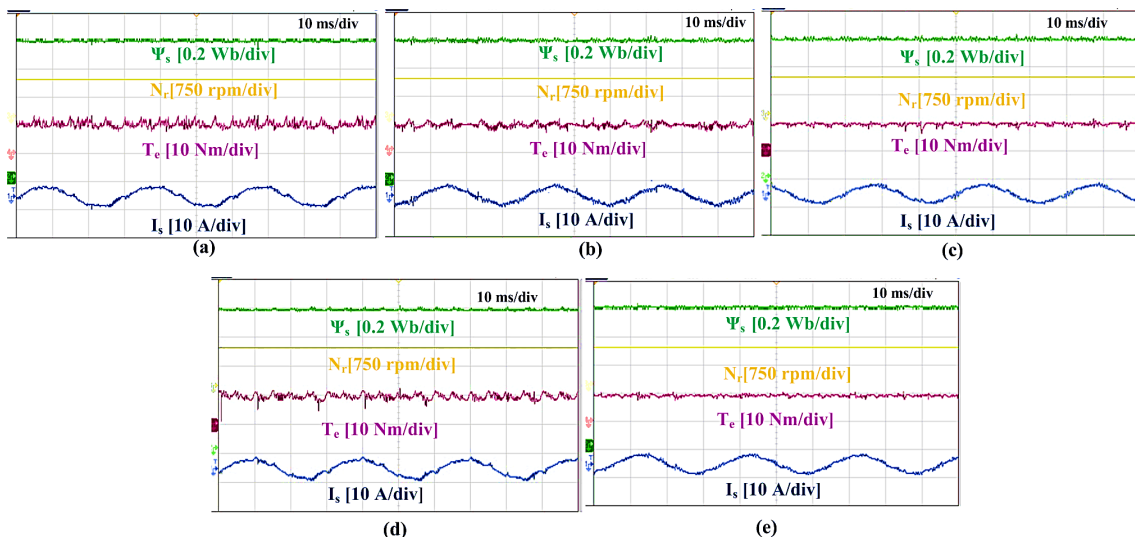


Fig.14. Steady-state drive performance at 1000 rpm and 10 Nm load when operated at equivalent switching frequency (a) BMPCC, (b) DBMPC[18], (c) MVBMPCC[27], (d) DBSVM[28] and (e) Proposed MPCC.

Table-IV. Performance indices at different speeds

Control scheme	500 rpm				750 rpm				1000 rpm			
	Torque ripple	Flux ripple	$f_{sw}(Hz)$	%THD	Torque ripple	Flux ripple	$f_{sw}(Hz)$	%THD	Torque ripple	Flux ripple	$f_{sw}(Hz)$	%THD
BMPCC	0.398	0.0022	2837	15.96	0.354	0.0022	2675	14.49	0.382	0.0019	2358	15.31
DBMPC[18]	0.298	0.0018	3812	13.48	0.282	0.0016	3712	11.25	0.287	0.0013	3389	10.25
MVBMPC[27]	0.231	0.0014	4329	9.82	0.185	0.0016	4521	8.07	0.243	0.0012	4451	7.72
DBDVM[28]	0.182	0.0010	10000	6.99	0.166	0.0010	10000	6.75	0.182	0.0010	10000	6.21
Proposed MPCC	0.214	0.0012	4325	7.28	0.172	0.0011	4431	7.54	0.216	0.0012	4266	6.79

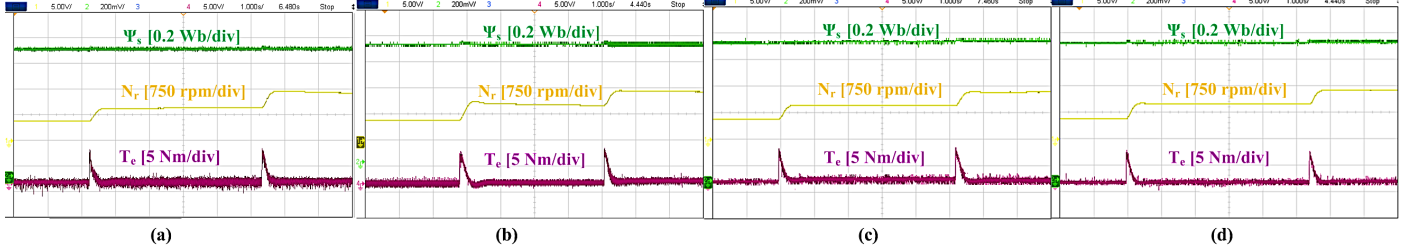


Fig.15. Dynamic acceleration from 450 rpm to 900 rpm to 1300 rpm (a) BMPCC, (b) DBMPC[18], (c) MVBMPC[27], (d) Proposed MPCC.

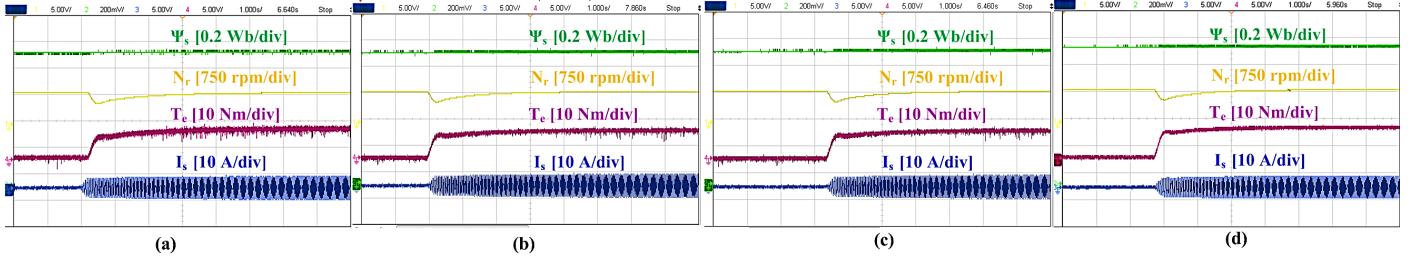


Fig.16. Dynamic load response when at 1000 rpm speed a load of 12 Nm is suddenly applied. (a) BMPCC, (b) DBMPC[18], (c) MVBMPC[27], (d) Proposed MPCC.

Table IV indicates the performance indices like the flux ripples, torque ripples, stator current total-harmonic distortion (THD) as well as the switching frequency (f_{sw}). From Table IV, it can be noticed that the proposed MPCC provides an enhanced steady-state torque response with lower distortion in stator current. The proposed scheme is less complex compared to DBMPC [18] and MVBMPC [27]. Thus, the steady-state responses validate the improved performance offered by the proposed method as multiple VVs are applied in every control period.

The dynamic performance of the proposed method is verified to further assert the effectiveness of the control scheme. The drive performance during acceleration, i.e., speed changes from 450 rpm to 900 rpm and then to 1300 rpm, is presented in Fig.

15. Correspondingly, the response during a sudden application of load from 0 to 50% of the rated load (12 Nm) at 1000 rpm speed is given in Fig. 16.

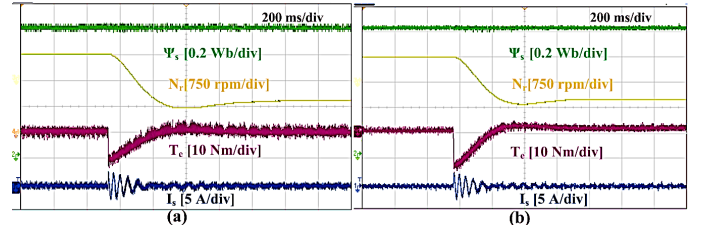


Fig.17. Dynamic response during speed reversal from 600 rpm to -600 rpm (a) BMPCC and (b) Proposed MPCC scheme.

Table V: Comparison of BMPCC, DBMPC[18], MVBMPC[27], DBSVM[28] and Proposed MPCC.

	BMPCC	DBMPC[18]	MVBMPC[27]	DBSVM [28]	Proposed method
Steady-state torque and flux ripples	0.38 Nm, 2.2 mWb	0.29 Nm, 1.8 mWb	0.2 Nm, 1.2 mWb	0.15 Nm, 1.2 mWb	0.17 Nm, 1.2 mWb
Switching frequency of the Inverter	2.6 kHz	3.7 kHz	4.5 kHz	10 kHz	4.5 kHz
Number of VVs used per sample	One	Two	Three	Three	Three
Number of steps involved in prediction, cost function evaluation and optimization	High 8 VVs	Low 2 VVs	Low 2 VVs	High 8 VVs	Low 2 VVs
Requirement of Sector determination	No	Yes	Yes	Yes	No
Effect of VVs on torque error, as well as flux error, considered during pre-selection	Yes	Yes	No	No	Yes
Calculation of reference VV	No	Yes	No	Yes	No
Computational Time (μs)	42	39	34	49.5	32.8
Implementation Complexity	Medium	High	Medium	High	Low
Dynamic response	Fast 0.3 s	Fast 0.3 s	Fast 0.3 s	Fast 0.3 s	Fast 0.3 s

Table VI: Computational time (t_{co})

Terms	BMPCC	DBMPC[18]	MVBMPC[27]	DBSVM[28]	Proposed method
	t_{co} (μ s)				
Measurement and estimation	8.12	8.12	8.12	8.12	8.12
Reference vector determination	-	1.46	-	1.46	-
Identification of the sector or VV selection criteria	-	13.07	13.07	2.1	0.8
Voltage vector grouping	-	5.96	1.31	-	2.2
Prediction and Cost Function Evaluation	24.23	4.57	-	24.23	12.85
Optimum vector determination	9.33	4.27	3.62	9.33	5.31
Duty ratio calculation	-	1.33	7.68	4.15	3.52
Total	42	39	34	49.5	32.8

The speed reversal response when reference speed is changed from 600 rpm to -600 rpm is shown in Fig. 17. Thus, all the dynamic responses affirm that the proposed scheme replicates the performance exhibited by the BMPCC scheme with an enhanced steady-state torque response. In the proposed scheme, the VV selection is based on the previous sample time VV and the direction of motor rotation. The VVs that can address all four stator current error conditions are included in the VVG. Moreover, the same VVG is used for the symmetrically opposite VVs. This reduces the computations involved in VVG assignments. The second optimum VV is also chosen based on minimum switching transitions. The amplitude optimization of the active VVs utilizes a simple duty-ratio calculation scheme. It involves fewer parameters and offers improved steady-state response as multiple VVs are applied. The computational complexity is not upsurged due to the proposed duty calculation.

C. Computational time

The computational burden of the control algorithm is estimated using the turnaround time of the algorithm, which is directly evaluated from the control desk of the dSPACE 1104. The BMPCC scheme uses 42 μ s time for its implementation using all the eight VVs in the control set. On the other hand, the two VV-based DBMPC [18] method requires 39 μ s for the algorithm implementation, whereas MVBMPC [27] uses 34 μ s and DBSVM[28] takes 49.5 μ s. On the contrary, the proposed method has an overall computational time of 32.8 μ s.

The advantages and disadvantages of the proposed scheme over BMPCC, DBMPC[18], and MVBMPC[27] can be summarized using Table V. Similarly, the computational time of all the methods is given in Table VI. The merit of the proposed method over the other schemes is that the VV preselection does not require any additional parameter determination. It is obtained from the previous VV applied and the direction of rotation of the machine. Moreover, the degree of freedom of control is improved with 4 VVs existing in every VVG for prediction, evaluation of cost function, and optimization steps. Further, the VVGs are the same for two symmetrically opposite VVs. This also helps to alleviate some computations associated with the preselection. In the DBMPC [18] scheme, the advantages of VV preselection are nullified due to the sector determination and reference VV calculation. The sectors are inevitably determined using the tangent inverse angle calculations. Similarly, in MVBMPC [27], the number of VVs used is limited to three. However, the VVs are grouped using the torque error and position of stator flux error. Moreover, the duty ratio calculation in MVBMPC [27] involves

more computations than the proposed scheme. Therefore, the proposed MPCC exhibits enhanced performance with a lesser burden on the digital processor.

V. CONCLUSION

An effective VV selection-based multivector MPCC method is proposed in this article for a 2L-VSI-fed PMSM drive. The optimum VV is obtained from a VVG framed using the VV applied in the previous control period and the direction of motor rotation. The VVs are grouped in such a way as to address all the error conditions. Thus, the VVs required for obtaining the optimum vector are limited to 4. The steady-state performance of the drive is enhanced by using three VVs in a sample time. The first VV to be applied is obtained from the VVG and the VV which yields the minimum cost function value is chosen as the optimum VV. Similarly, VV adjacent to the first optimum VV is selected as the next optimum VV. The second VV is determined based on an improved position assessment of stator VV error using simple relational operations. This helps to limit the switching transitions. The proposed scheme avoids the sector determination, and the stator voltage error is obtained from the stator current error and a constant. This ensures reduced sensitivity to machine parameter variations. Further, the proposed duty ratio calculation does not induce additional complexity in the algorithm. The steady-state torque performance is enhanced without enlarging the computational time while replicating the dynamic performance exhibited by the BMPCC scheme.

REFERENCES

- [1] T. Li, X. Sun, G. Lei, Y. Guo, Z. Yang, and J. Zhu, "Finite-Control-Set Model Predictive Control of Permanent Magnet Synchronous Motor Drive Systems—An Overview," *IEEE/CAA Journal of Automatica Sinica*, vol. 9, no. 12, pp. 2087–2105, December 2022.
- [2] C. Liu, "Emerging electric machines and drives—An overview," *IEEE Trans. Energy Convers.*, vol. 33, no. 4, pp. 2270–2280, Dec. 2018.
- [3] Feng Niu, Bingsen Wang, Andrew S. Babel, Kui Li, and Elias G. Strangas, "Comparative Evaluation of Direct Torque Control Strategies for Permanent Magnet Synchronous Machines," *IEEE Trans. Power Electron.*, vol. 31, no. 2, pp. 1408–1424, Jan. 2016.
- [4] J. Rodriguez, R. M. Kennel, J. R. Espinoza, M. Trincado, C. A. Silva, and C. A. Rojas, "High-performance control strategies for electrical drives: An experimental assessment," *IEEE Trans. Ind. Electron.*, vol. 59, no. 2, pp. 812–820, Feb. 2012.
- [5] D. Casadei, F. Profumo, G. Serra, and A. Tani, "FOC and DTC: two viable schemes for induction motors torque control," *IEEE Trans. Power Electron.*, vol. 17, no. 5, pp. 779–787, Sep. 2002.
- [6] J. Rodriguez *et al.*, "State of the art of finite CS model predictive control in power electronics," *IEEE Trans. Ind. Informat.*, vol. 9, no. 2, pp. 1003–1016, May 2013.

- [7] S. Vazquez, J. Rodriguez, M. Rivera, L. G. Franquelo, and M. Norambuena, "Model predictive control for power converters and drives: Advances and trends," *IEEE Trans. Ind. Electron.*, vol. 64, no. 2, pp. 935–947, Feb. 2017.
- [8] E. Kusuma, K. M. R. Esvar and T. V. Kumar, "An Effective Predictive Torque Control Scheme for PMSM Drive without Involvement of Weighting Factors," *IEEE Journal of Emerging and Selected Topics in Power Electronics*, vol. 9, no. 3, pp. 2685–2697, June 2021.
- [9] Y. Zhang, D. Xu, and L. Huang, "Generalized Multiple-Vector-Based Model Predictive Control for PMSM Drives," *IEEE Trans. Ind. Electron.*, vol. 65, no. 12, pp. 9356–9366, Dec. 2018.
- [10] Y. Zhang, D. Xu, J. Liu, S. Gao, and W. Xu, "Performance Improvement of Model-Predictive Current Control of Permanent Magnet Synchronous Motor Drives," *IEEE Trans. Ind. Appl.*, vol. 53, no. 4, pp. 3683–3695, Aug. 2017.
- [11] X. Zhang, L. Zhang, and Y. Zhang, "Model Predictive Current Control for PMSM Drives With Parameter Robustness Improvement," *IEEE Trans. Power Electron.*, vol. 34, no. 2, pp. 1645–1657, Feb. 2019.
- [12] Y. Zhang, Y. Bai and H. Yang, "A Universal Multiple-Vector-Based Model Predictive Control of Induction Motor Drives," *IEEE Trans. Power Electron.*, vol. 33, no. 8, pp. 6957–6969, Aug. 2018.
- [13] X. Li, Z. Xue, X. Yan, L. Zhang, W. Ma, and W. Hua, "Low-Complexity Multivector-Based Model Predictive Torque Control for PMSM With Voltage Preselection," *IEEE Trans. Power Electron.*, vol. 36, no. 10, pp. 11726–11738, Oct. 2021.
- [14] M. L. Parvathy and V. K. Thippiripati, "An Effective Modulated Predictive Current Control of PMSM Drive With Low Complexity," *IEEE Journal of Emerging and Selected Topics in Power Electronics*, vol. 10, no. 4, pp. 4565–4575, Aug. 2022.
- [15] Z. Zhang, H. Fang, F. Gao, J. Rodríguez and R. Kennel, "Multiple-Vector Model Predictive Power Control for Grid-Tied Wind Turbine System With Enhanced Steady-State Control Performance," *IEEE Trans. Ind. Electron.*, vol. 64, no. 8, pp. 6287–6298, Aug. 2017.
- [16] M. Mamdouh and M. A. Abido, "Efficient Predictive Torque Control for Induction Motor Drive," *IEEE Trans. Ind. Electron.*, vol. 66, no. 9, pp. 6757–6767, Sept. 2019.
- [17] J. Chen, Y. Qin, A. M. Bozorgi and M. Farasat, "Low Complexity Dual-Vector Model Predictive Current Control for Surface-Mounted Permanent Magnet Synchronous Motor Drives," *IEEE Journal of Emerging and Selected Topics in Power Electronics*, vol. 8, no. 3, pp. 2655–2663, 2020.
- [18] X. Zhang and B. Hou, "Double vectors model predictive torque control without weighting factor based on voltage tracking error," *IEEE Trans. Power Electron.*, vol. 33, no. 3, pp. 2368–2380, March 2018.
- [19] M. L. Parvathy and T. V. Kumar, "A Multivector-Based Model Predictive Current Control of PMSM Drive With Enhanced Torque and Flux Response," *IEEE Journal of Emerging and Selected Topics in Power Electronics*, vol. 10, no. 6, pp. 7527–7538, Dec. 2022.
- [20] Y. Zhang and H. Yang, "Two-vector-based model predictive torque control without weighting factors for induction motor drives," *IEEE Trans. Power Electron.*, vol. 31, no. 2, pp. 1381–1390, Feb. 2016.
- [21] M. Xiao, T. Shi, Y. Yan, W. Xu, and C. Xia, "Predictive torque control of permanent magnet synchronous motors using flux vector," *IEEE Trans. Ind. Appl.*, vol. 54, no. 5, pp. 4437–4446, Sep./Oct. 2018.
- [22] Z. Zhou, C. Xia, Y. Yan, Z. Wang, and T. Shi, "Torque Ripple Minimization of Predictive Torque Control for PMSM With Extended Control Set," *IEEE Trans. Ind. Electron.*, vol. 64, no. 9, pp. 6930–6939, Sep. 2017.
- [23] Z. Chen and J. Qiu, "Adjacent-Vector-Based Model Predictive Control for Permanent Magnet Synchronous Motors with Full Model Estimation," *IEEE Journal of Emerging and Selected Topics in Power Electronics*, doi: 10.1109/JESTPE.2022.3172714.
- [24] H. Yang, Y. Zhang, and M. Li, "Duty-Cycle Correction-based Model Predictive Current Control for PMSM Drives Fed by a Three-level Inverter with Low Switching Frequency," *IEEE Trans. Power Electron.*, doi: 10.1109/TPEL.2023.3250480.
- [25] B. Yu, W. Song, Y. Guo, J. Li and M. S. R. Saeed, "Virtual Voltage Vector-Based Model Predictive Current Control for Five-Phase VSIs With Common-Mode Voltage Reduction," *IEEE Trans. Transp. Electrification*, vol. 7, no. 2, pp. 706–717, June 2021.
- [26] C. L. Xia, S. Wang, Z. Wang, and T. Shi, "Direct torque control for VSI-PMSMs using four-dimensional switching-table," *IEEE Trans. Power Electron.*, vol. 31, no. 8, pp. 5774–5785, Nov. 2016.
- [27] X. Li, Z. Xue, L. Zhang and W. Hua, "A Low-Complexity Three-Vector-Based Model Predictive Torque Control for SPMSM," *IEEE Trans. Power Electron.*, vol. 36, no. 11, pp. 13002–13012, Nov. 2021.
- [28] X. Ba, P. Wang, C. Zhang, J. G. Zhu and Y. Guo, "Improved Deadbeat Predictive Current Control to Enhance the Performance of the Drive System of Permanent Magnet Synchronous Motors," *IEEE Transactions on Applied Superconductivity*, vol. 31, no. 8, pp. 1–4, Nov. 2021.
- [29] C. Zhang et al., "Model-Free Predictive Voltage Control of the Floating Capacitor in Hybrid-Inverter Open-Winding Permanent Magnet Synchronous Motor," *IEEE Trans. Ind. Electron.*, vol. 71, no. 10, pp. 11925–11935, Oct. 2024.
- [30] E. Zafra, S. Vazquez, A. M. Alcaide, L. G. Franquelo, J. I. Leon and E. P. Martin, "K-Best Sphere Decoding Algorithm for Long Prediction Horizon FCS-MPC," *IEEE Trans. Ind. Electron.*, vol. 69, no. 8, pp. 7571–7581, Aug. 2022.
- [31] M. S. R. Saeed, W. Song, B. Yu, Z. Xie and X. Feng, "Low-Complexity Deadbeat Model Predictive Current Control for Open-Winding PMSM Drive With Zero-Sequence Current Suppression," *IEEE Trans. Transp. Electr.*, vol. 7, no. 4, pp. 2671–2682, Dec. 2021.
- [32] C. Zhang, C. Gan, K. Ni, Z. Yu, S. Wang and R. Qu, "Computationally Efficient Cascaded Predictive Control for Hybrid-Inverter Fed Open-Winding PMSM Drive With Fast Partial Preselection" *IEEE Trans. Power Electron.*, vol. 39, no. 3, pp. 3509–3520, March 2024.
- [33] Y. Chen, X. Wang, D. Xiao, D. Ma, X. Yang and Z. Wang, "Model Predictive Control of Five-Level Open-End Winding PMSM Drives," *IEEE Trans. Transp. Electr.*, vol. 10, no. 4, pp. 10115–10124, Dec. 2024.
- [34] M. S. R. Saeed, W. Song, L. Huang and B. Yu, "Double-Vector-Based Finite Control Set Model Predictive Control for Five-Phase PMSMs With High Tracking Accuracy and DC-Link Voltage Utilization," *IEEE Trans. Power Electron.*, vol. 37, no. 12, pp. 15234–15244, Dec. 2022.
- [35] X. Wu, Y. Wang, N. Wang, H. Xing, W. Xie and C. H. T. Lee, "A Novel Double-Vector Model Predictive Current Control for PMSM With Low Computational Burden and Switching Frequency," *IEEE Trans. Power Electron.*, doi: 10.1109/TPEL.2025.3542793.
- [36] K. Huang et al., "An Extended Model Predictive Control for PMSM With Minimum Ripples and Small Runtimes," *IEEE Trans. Ind. Electron.*, doi: 10.1109/TIE.2025.3531467.



Parvathy M.L. received the B.Tech. and M.Tech. degrees in Electrical Engineering from the University of Kerala, India, in 2014 and 2017, respectively. She received her Ph.D. degree from the Department of Electrical Engineering, National Institute of Technology, Warangal, India, in 2023.

She is currently working as a Postdoctoral Research Associate in Power Electronics at Durham University, United Kingdom. Her research interests include power electronics, control of electrical drives, specifically model predictive control schemes and DC-DC converters and their control.



Vinay Kumar Thippiripati was born in Kadapa, India, in 1984. He received the B.Tech. and M.Tech. degrees in Electrical Engineering from Jawaharlal Nehru Technological University, Hyderabad, India, in 2005 and 2008, respectively. He received the Ph.D. degree in Electrical Engineering from the National Institute of Technology, Warangal, India, in 2015.

In 2013, he joined in National Institute of Technology, Warangal, India, as an Assistant Professor. His research interests include power electronics and drives, direct torque control, predictive torque control, open-end winding induction motor drives, multilevel inverters, hybrid electric vehicles, and renewable energy interfacing.



Citation on deposit:

Mohanan Leela, P., & Thippiripati, V. K. (in press).
An Effective Multivector Model Predictive Current
Control for PMSM Drive based on Low-
Complexity Voltage Vector Preselection. IEEE

Journal of Emerging and Selected Topics in Circuits and Systems,

For final citation and metadata, visit Durham Research Online URL:

<https://durham-repository.worktribe.com/output/4090588>

Copyright statement:

This accepted manuscript is licensed under the Creative Commons Attribution
licence. <https://creativecommons.org/licenses/by/4.0/>